

2-2 Optical Amplification and Switches in Silicon Based Photonic Devices for Future Networks

T.K. Liang, L.R. Nunes, H.K. Tsang, and TSUCHIYA Masahiro

Silicon photonics technology has attracted immense research interest because it offers low cost optoelectronics solutions for telecommunications applications. In silicon-on-insulator optical waveguides, light is confined in a single-crystal silicon layer separated from the substrate by a thin layer of buried silicon dioxide. The large step in refractive index enables a tight confinement of light in a small waveguide area, which can be exploited to achieve high optical intensity propagation. Thus many practical nonlinear optical devices can be realized in these waveguides. In this paper, we study the optical nonlinearities in silicon waveguides, including two-photon absorption, free-carrier absorption and stimulated Raman scattering. Several silicon-based photonic devices have been developed for future communications systems, including waveguide two-photon absorption autocorrelator, ultrafast optical silicon optical switches and waveguide optical Raman amplifier.

Keywords

Silicon photonics, Optical switch, Optical amplifier, Photonic devices

1 Introduction

Silicon has attracted immense interest as a material for photonic devices[1] because of its low loss at wavelengths used in optical communications and the availability of mature processing technologies developed for the microelectronics industry. Practical applications of silicon in photonics has been largely limited to passive devices because the indirect band-gap of silicon makes it inefficient in converting electric current to light. The development of active devices using silicon has been a major challenge that has prompted much research such as silicon nanocrystals[2] and silicon-germanium superlattices[3].

In silicon-on-insulator optical waveguides, light is confined in a single-crystal silicon layer separated from the substrate by a thin layer of buried silicon dioxide. The large step

in refractive index enables a tight confinement of light in a small waveguide area. The small mode area of the silicon waveguide allows high peak optical intensity propagation and lead to the manifestation of nonlinear optical effects. Thus many practical nonlinear optical devices can be realized in these waveguides. Nonlinear optical properties such as two-photon absorption (TPA) and free-carrier absorption (FCA) of SOI waveguides need to be accurately characterized. Recently, stimulated Raman scattering in silicon waveguides[4] was shown to have potential for light amplification because the Raman coefficient of silicon is several orders of magnitude larger than silica[5].

Sub-micron size silicon waveguides (or called wire waveguides) are possible because of the extremely high index contrast ($n=3.5$ for silicon, and $n=1.45$ for SiO_2), which allows

the dimension of waveguides to be much smaller than in conventional low index contrast silica waveguides. The strong optical confinement and small effective modal area ($<0.1 \mu\text{m}^2$) of such waveguides can produce high optical intensities even at input optical powers typically used in telecommunications. The high optical intensities and long interaction lengths in the waveguides allow nonlinear optical effects to be readily apparent. Apart from other nonlinear optical devices such as optical fibers and semiconductor optical amplifiers, silicon wire waveguides have good potential for other nonlinear devices for ultrafast photonics signal processing.

2 Optical nonlinearities in silicon

2.1 Two photon absorption (TPA)

Silicon has an indirect bandgap of 1.1 eV (or $1.1 \mu\text{m}$). The photons at telecommunication wavelength band of $1.55 \mu\text{m}$, with energy of 0.8 eV, do not have sufficient energy to be absorbed in crystalline silicon. However, if the optical intensity is high enough, two photons will be absorbed simultaneously and create electron-hole pairs in the crystal [6]. This nonlinear optical effect is called two-photon absorption (TPA). TPA is detrimental for ultrafast all-optical switches because of the reduction in switching speed caused by the long-lived carriers and the limiting action of TPA on pump power. The presence of a large TPA coefficient restricts the usefulness of semiconductor material for all optical switching to those which operate below half the bandgap energy [7]. In this section, the measurement of TPA coefficient in the SOI waveguides is described.

The propagation loss of light along the waveguide due to linear absorption and TPA can be described by

$$\frac{dI}{dz} = -\alpha I - \beta_2 I^2 \quad (1)$$

where z is the propagation direction, α is the linear absorption, I is the optical intensity and β_2 is the TPA coefficient.

Figure 1 shows the experimental setup for TPA coefficient measurements and the waveguide structure. The pigtailed silicon waveguide used in the experiment had a fiber-to-fiber insertion loss of 1 dB, an effective area of $6.2 \mu\text{m}^2$ and a length of 1.7 cm. The linear loss of the waveguide was 0.1 dB/cm. A distributed feedback (DFB) laser, gain-switched by an electrical impulse generator, was used to produce 40 ps optical pulses with 1 MHz repetition rate. The operating wavelength of the laser (1547 nm) was well below the indirect bandgap of silicon such that linear absorption was negligible. The optical pulses were then amplified by a high power erbium-doped fiber amplifier (EDFA) and a variable optical attenuator (VOA) controlled the input power. A small amount (5%) of incident optical power was split out by an optical coupler to monitor the input power.

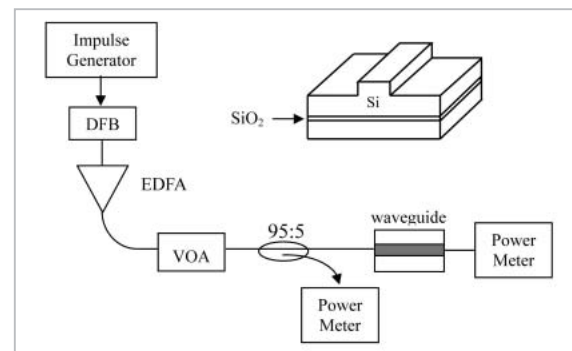


Fig. 1 TPA measurement setup and waveguide structure

DFB: distributed feedback laser, VOA: variable optical attenuator

At high peak power, TPA became detrimental and limited the maximum transmitted power. By varying input powers, reciprocal of transmission $1/T$ against incident optical power was plotted in Fig. 2. The ratio of input power to output power (i.e. $1/T$) and the TPA coefficient, are related by [8]

$$\frac{1}{T} = \exp(\alpha L) \frac{\beta_2 L_{eff}}{A_{eff}} P_i + \exp(\alpha L) \quad (2)$$

where A_{eff} is the effective area of optical mode field profile, P_i is the input power and L_{eff} is the effective length, described by $[1 - \exp(-\alpha L)]/\alpha$.

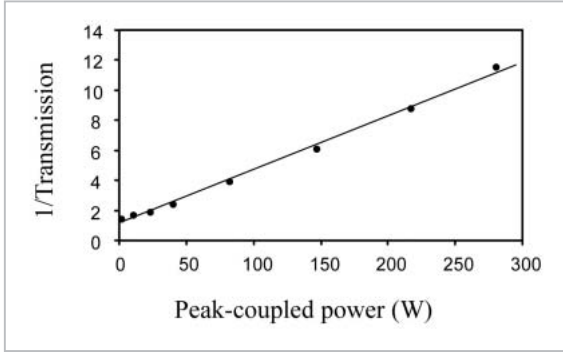


Fig.2 Reciprocal transmission versus peak-coupled power

The TPA coefficient β_2 , determined by the slope of the curve in Fig. 2, was found to be 6.7×10^{-12} m/W and the measurement error was estimated to be $\pm 10\%$.

In the measurement, the low fiber-to-fiber insertion loss allowed accurate estimation of peak-coupled power. Hence the measured β_2 is more accurate than before and the value is consistent with the recent independent measurement[9] using the Z-scan method. The effects of free-carrier absorption from carriers generated by TPA were neglected in our measurement of TPA coefficient. TPA generated carriers will introduce additional optical loss which however is only significant if there is both a large TPA coefficient and a long integration time (long pulsewidth). In our measurements, the repetition rate of the pulse train was sufficiently low to allow carriers generated by previous pulses to have enough time to recombine.

2.2 Free carrier absorption (FCA)

Once photons are absorbed in silicon waveguides due to TPA, excess electron-hole pairs or free carriers will be generated. The small waveguide area confine these free carriers and lead to high carrier concentration. The excess loss from TPA generated free carriers in silicon waveguides may be estimated by quantifying the number of carriers generated from the incident pump power. The analysis below is based on the assumption of continuous-wave (CW) operated optical source, which is actually what was used as the pump source for Raman scattering experiments in

later sections.

Based on equation (1), the total optical power absorbed due to TPA along the waveguide (z-direction) may be described as

$$P_{tpa}(z) = \frac{\beta_2}{A_{eff}} \int_0^z P^2(z) dz \quad (3)$$

For every two photons absorbed inside the waveguide, an electron-hole pair (EHP) will be generated. The EHP generation rate is described as

$$\frac{dN}{dt} = \frac{P_{tpa}(z)}{2h\nu} - \frac{N}{\tau_c} \quad (4)$$

where N is the number of electrons/holes, $h\nu$ is the photon energy and τ_c is the free carrier relaxation time due to e-h recombination and carrier diffusion.

Once we know the number of electrons/holes, we can calculate carrier density inside the waveguide. Carrier density calculation is non-trivial because of nonlinear effects such as carrier density dependent carrier lifetimes and mobilities. Finally, free-carrier absorption coefficient α_{fca} can be approximated using the classical Drude model[10].

$$\alpha_{fca}(z) = \frac{q^3 \lambda^2}{4\pi^2 c^3 \epsilon_0 n} \left(\frac{N_e(z)}{m_e^2 \mu_e} + \frac{N_h(z)}{m_h^2 \mu_h} \right) \quad (5)$$

where $N_e(z)/N_h(z)$ is the free carrier density, n is the refractive index of silicon, q is the electron charge, ϵ_0 is free-space permittivity, c is the light velocity in vacuum, m_e/m_h is the effective mass and μ_e/μ_h is the free carrier mobility, subscripts e and h denote electrons and holes respectively. A typical graph of carrier induced optical loss is plotted in Fig. 3. Optical power transmitted through waveguide is attenuated by the injected free carriers via p-i-n diode structure.

2.3 Stimulated raman scattering (SRS)

Because of the crystal symmetry, silicon is generally believed to be void of useable nonlinear properties. While the symmetry does prohibit 2nd order nonlinearities in bulk silicon, 3rd order phenomena do exist. Typically, 3rd order nonlinearities are too weak to be

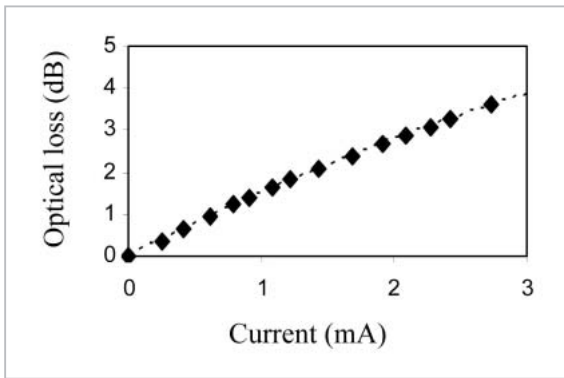


Fig.3 Optical loss at different injected current levels

practical in integrated optical devices, because of their small sizes. One interesting exception is the Raman scattering. The Raman gain coefficient in silicon is several orders of magnitude larger than that in the amorphous glass fiber because of the single crystal structure. In addition, the tight optical confinement in an SOI waveguide will lower the threshold for Stimulated Raman Scattering (SRS).

Figure 4 shows the experimental setup for SRS measurements. The waveguide used has pn doping on two sides of the rib area to form a p-i-n diode structure. The pump sources were two polarization multiplexed Raman pump diode lasers. Both pump lasers operated at 1440 nm and the maximum output power of each laser was 400 mW. The 3-dB spectral width of the pump laser was 1 nm. A tunable laser (linewidth < 200 kHz) was used as the

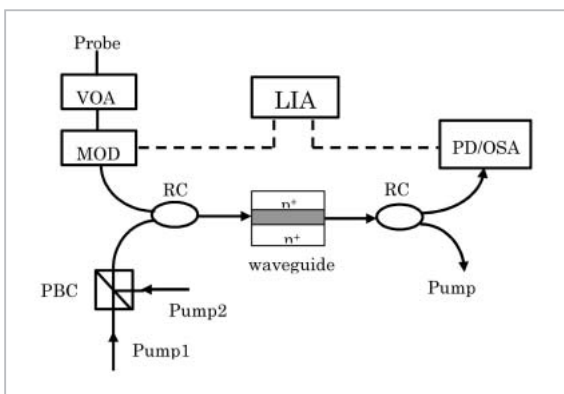


Fig.4 Experimental setup

LIA: lock-in amplifier, RC: Raman coupler, PD: photodiode, OSA: optical spectrum analyser, PBC: polarization beam combiner, MOD: modulator.

probe signal at Stokes wavelength range to measure the SRS. Both pump and probe signal were combined by a Raman coupler then coupled into the waveguide through a short length of optical fiber. Another Raman coupler was used to separate the two different wavelength signals after the waveguide. Standard lock-in technique was employed to improve the signal to noise rejection of the detected probe signal. An optical modulator imposed 200 Hz amplitude modulation on the probe signal to give a reference frequency for the lock-in amplifier (LIA). Because the modulation was applied on the probe signal, the LIA detected the probe signal power variation when the pump light was introduced into the waveguide.

Spontaneous Raman scattering was readily observed at the Stokes wavelength (Fig. 5) using an optical spectrum analyzer (OSA). Spectral measurements of the spontaneous Raman emission near the Stokes wavelength of 1556.5 nm (corresponding to first order Raman scattering shift of 15.6 THz) were made at a total pump power of 570 mW with the optical spectrum analyzer set to a resolution of 0.1 nm.

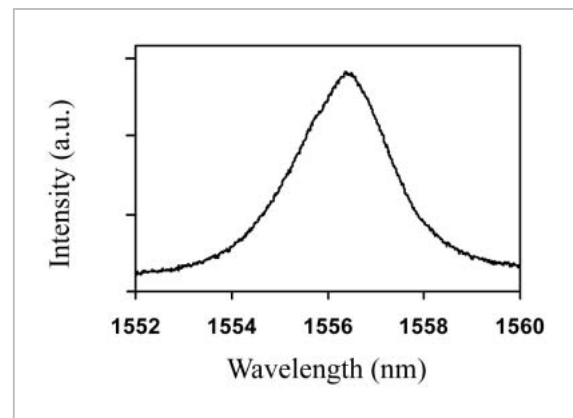


Fig.5 Spontaneous Raman spectrum of silicon waveguides

Contrary to initial expectations, we observed that the probe power fell when the pump power was increased. Shown in Fig. 6 are the normalized transmission curves at two probe wavelengths — 1550.5 nm (circle) and the peak Stokes wavelength at 1556.5 nm (triangle). 100% transmission was defined as the

transmission without any pump power. The waveguide had over 20% pump induced loss when the p-n diode was open circuit (Fig. 6a), and the excess loss was reduced to less than 7% (Fig. 6b) when the p-n diode structure was electrically short-circuited. The observed results may be explained by the presence of TPA generated excess carriers inside the waveguide. The TPA generated e-h pairs are confined to the rib region by the geometry of the etched doping holes on either side of the rib and the build up of electric charge from photogenerated carriers at the p and n regions. As a result, carrier density in the rib is high and free carrier absorption is significant in the waveguide. When the p-n diode was short-circuited (or reverse biased), the external circuit provided a path for the photogenerated carriers to flow out of rib region and thus reduced the optical loss measured for the short circuit waveguide compared with the open circuit waveguide.

The probe signal at the Stokes wavelength 1556.5 nm experienced less net loss despite the presence of stimulated Raman scattering because of the free carrier absorption. The spectral dependence of the stimulated Raman scattering was obtained by scanning probe signal wavelength at a fixed coupled pump power of 570 mW (shown in Fig. 7). Relative “gains” of 1.7% (Fig. 7a) and 2.1% (Fig. 7b) were obtained at 1556.5 nm through stimulated Raman scattering for the open circuit and short circuit waveguides respectively. However, the overall losses from free-carrier absorption were greater than the Raman gain in both cases. The SRS gain spectrum is consistent with the spontaneous Raman scattering measured by optical spectrum analyzer.

The explanation that the pump induced excess loss was caused by free carriers generated from two-photon absorption, was further supported by the observation that the photocurrent measured by the p-n diode contacts

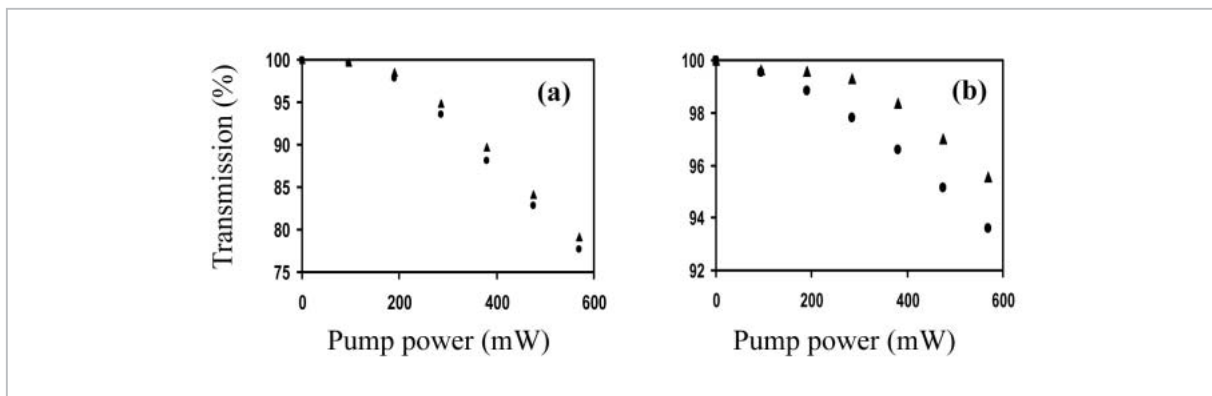


Fig.6 Normalized transmission of probe signals at different coupled pump powers (a) p-n diode open circuit, (b) p-n diode short circuit. Triangle: 1556.5 nm, Circle: 1550.5 nm.

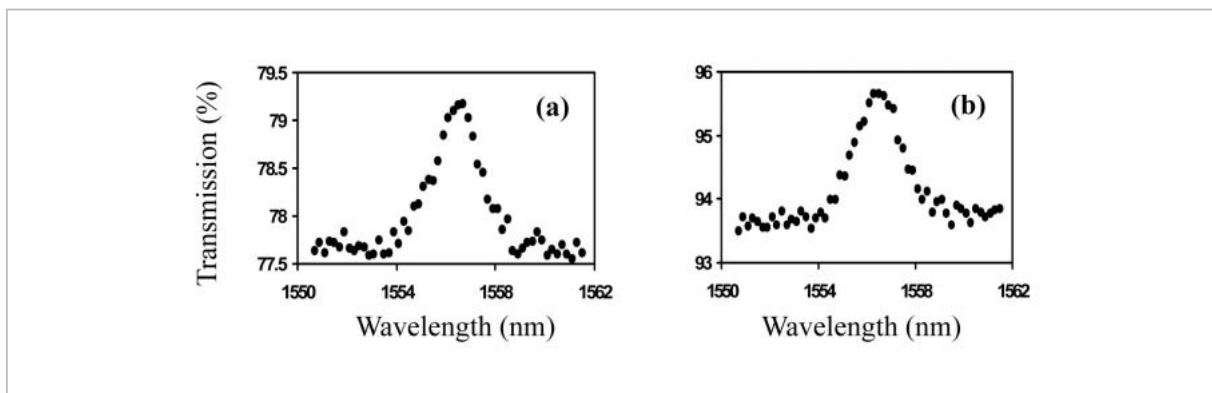


Fig.7 Stimulated Raman scattering measurement (a) open-circuit, (b) short-circuit across p-n diode.

at either side of the rib waveguide varied quadratically with pump power. The TPA coefficient of silicon is much smaller than for InP/InGaAsP waveguides [8] because only phonon-assisted two-photon transitions are possible. Because of the small magnitude of the TPA coefficient in the SOI waveguide, the intrinsic loss of pump power due to TPA can be neglected. However, the excess loss arising from TPA generated carriers is quite significant and increases with the pump power. This effect put a serious limitation in realizing a silicon waveguide Raman amplifier. Deliberate measures have to be applied to reduce the effect of TPA generated free carrier absorption. Other alternatives, such as ion implantation to increase carrier recombination rates or using ultra-short pulses as the pumping source, to reduce the carrier density are also possible.

3 Applications of silicon waveguides

3.1 Autocorrelation detector

Optical autocorrelation for measuring ultra-short laser pulses [11] typically involves splitting an ultrashort laser pulse, adding a variable relative time delay between the split pulse components before their recombination at a nonlinear crystal (with the correct crystal orientation for phase-matching) for second harmonic generation (SHG) which can be measured by a photomultiplier (PM) tube. TPA in semiconductors is an attractive alternative to SHG for autocorrelation [12]-[14] because of potential lower cost (compared to the use of PM tube detectors), increased sensitivity and ease of use resulting from having a wide wavelength range of operation without needing the adjustment of crystal tilt angle for phase matching of a nonlinear crystal for SHG. In this section, we study the use of a silicon waveguide for TPA autocorrelation. The large direct bandgap of silicon makes direct two-photon absorption energetically impossible, but indirect two-photon transition are present and the long interaction lengths possible

in an optical waveguide provide easily detectable photocurrents from TPA.

Figure 8 shows the structure of the silicon waveguide used in the experiments. P-type and n-type dopants were implanted beside the rib region to form a *p-i-n* diode structure and ohmic contacts were made to the doped areas.

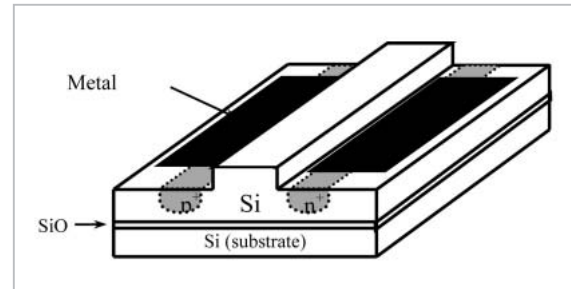


Fig.8 Structure of the silicon waveguide autocorrelator

A single beam measurement of the TPA photoconductivity was carried out initially. Polarized (TE) picosecond optical pulses, produced from a passive mode-locked fiber ring laser were end-fire coupled into the waveguide via an objective lens. The *p-i-n* diode structure was reverse biased to sweep out the free carriers generated inside the waveguide. The incident optical power was then varied to different values with an optical attenuator at this bias. The measured photocurrent showed a quadratic dependence on the coupled power (Fig. 9), consistent with TPA-induced photocurrent generation inside the waveguide.

The experimental setup for the silicon waveguide autocorrelator demonstration is shown in Fig. 10. The incident beam was firstly collimated by a 10 X objective lens. The

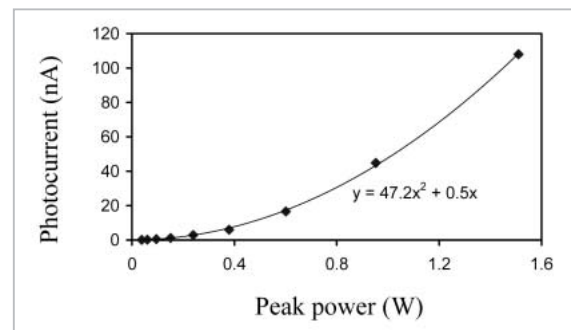


Fig.9 Measured photocurrent against optical peak power

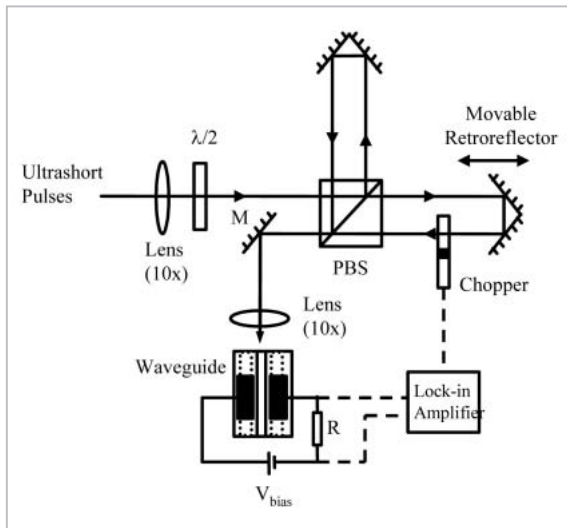


Fig. 10 Experimental setup of autocorrelation measurement

PBS: polarization beam splitter, R: biasing resistor, M: mirror.

polarization beam splitter (PBS) then divided the incident beam into two orthogonal polarized beams. The half-wave plate controlled the optical power ratio of the two beams. The movable retroreflector provided a finely adjustable optical delay in one of the path. An optical chopper was placed at the same path to provide modulation on the input light beam. This allowed a lock-in amplifier to accurately measure the photocurrent generated inside the waveguide. The recombined optical pulses were then end-fire coupled into the waveguide through a 10 X objective lens. Two current probes were placed on the top of the metal contacts of p-type and n-type doping regions respectively to detect the photocurrent.

Figure 11 shows the autocorrelation trace of the laser pulse obtained by the silicon waveguide. The measured photocurrent has been averaged over a suitable period of time in the lock-in amplifier to obtain a smooth trace. The full width half maximum (FWHM) autocorrelation width of TPA signal was 2.1 ps, which was corresponding to 1.35 ps pulsewidth for a real hyperbolic secant pulse. The temporal profile of the pulse was coincident with the result obtained by the conventional SHG autocorrelation after background calibration. To verify the performance of the

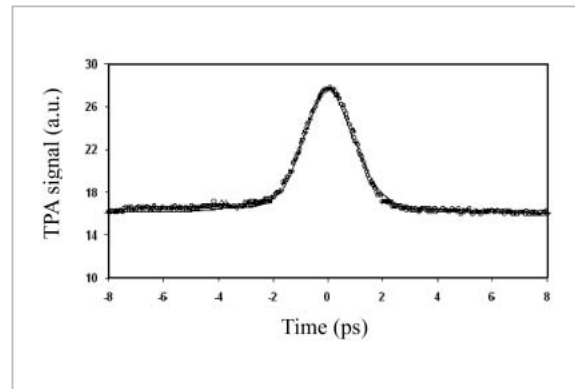


Fig. 11 Autocorrelation traces obtained by silicon waveguide

silicon waveguide autocorrelator, the output pulses from passive mode-locked fiber ring laser was amplified in a standard erbium-doped fiber amplifier (EDFA). The pulses were compressed (~ 530 fs FWHM) due to self-phase modulation (SPM) and dispersion of the fiber in the EDFA. Again, the autocorrelation trace obtained by silicon waveguide was in good agreement with the one obtained by SHG autocorrelation.

Since the bandgap of silicon is at 1.1 eV, the spectral operating range of the TPA autocorrelator is expected to be from $1.1 \mu\text{m}$ to $2.2 \mu\text{m}$ wavelength. Two photons have insufficient energy to excite interband transition beyond $2.2 \mu\text{m}$. The sensitivity of the silicon waveguide autocorrelator was measured by inserting an optical attenuator in the incident beam path to reduce the optical power inside the waveguide. The sensitivity of the silicon waveguide autocorrelator, defined as the product of the peak and average power of the minimum detectable signal, was found to be 1 mW^2 . This value is similar to that of a conventional SHG autocorrelator [15] and higher than that of silicon avalanche photodiode [16].

3.2 Ultrafast optical switches

There is much research interest in all-optical nonlinearities in semiconductor optical waveguide because of their prospect in all-optical switches for future ultrafast photonics signal processing devices [17]. Two-photon absorption (TPA) is widely acknowledged to

degrade the performance of switching devices in III - V semiconductor waveguides. TPA is itself an instantaneous effect, but it results in the generation of electron-hole pairs, whose lifetime limits the device speed by means of secondary effects, such as free carrier absorption (FCA) or plasma dispersion effect. Therefore, ultra-fast switching is possible if one can make use of the former instantaneous effect while simultaneously suppressing other secondary effects. In recent years, the advancement of nanoscale fabrication technology allows the realization of low loss (<0.2 dB/mm) submicron size silicon wire waveguides[18]. The strong optical confinement and small effective modal area ($<0.1 \mu\text{m}^2$) of such waveguides can produce high optical intensities even at input optical powers typically used in telecommunications. The high optical intensities and long interaction lengths in the waveguides allow nonlinear optical effects to be readily apparent. Many kinds of silicon waveguide based optical switches have been reported so far[19]. Among them, the switching mechanisms in most of the devices are based on plasma dispersion effect. However, the switching speed is always limited by the effective carrier lifetime, which is typically in the ranges of hundreds of picoseconds for wire waveguides[20] and nanoseconds in silicon rib waveguides[21]. In this section, we demonstrate all-optical switching using non-degenerate TPA process inside silicon wire waveguides. Our results showed that the direct use of TPA allows operation speeds which are not limited by the slow effective carrier lifetime in the silicon wire waveguides.

A two-color time-resolved pump probe experiment was performed to measure the nonlinear transmission of weak probe pulses in the presence of strong optical pump pulses in silicon wire waveguides. The waveguide sample used in the experiment was formed by a silicon stripe measuring 480 nm by 220 nm on silicon-on-insulator wafer with device length of 10 mm, as shown in Fig. 12(a). Both pump and probe pulses were generated by the spectral slicing of a broadband stretched pulse

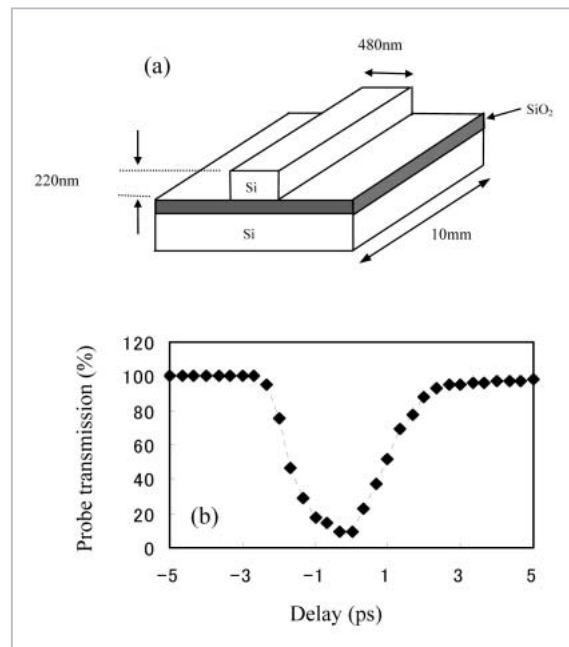


Fig. 12 (a) Wire waveguide structure (b) Time-resolved probe transmission in cross-correlation measurement

passive mode-locked fiber laser operating near 1550 nm wavelength. Pump and probe pulses were selected at two different wavelengths to avoid interference and ensure a stable measurable result. The repetition rate of the pulse source was 50 MHz. The time separation between the pump pulses (20 ns) are sufficient long, such that all the photo-generated free carriers have enough time to recombine. Both FWHM pulsewidths of the pump and probe pulses were measured to be 1.5 ps by an auto-correlator.

In Fig. 12(b), the measured signal transient around zero delay time represents a cross correlation curve between pump and probe pulses. The recovery time of the probe signal was less than 3 ps, indicating that the device can operate at high speed. The probe transmission recovered to more than 90% showing that there was no significant accumulation of free carriers inside the waveguide.

Shown in Fig. 13 is the modulation depth of the probe pulse as a function of pump peak powers. The modulation of the probe pulse is more than 90% when the pump peak power is greater than 5 W. However, the maximum

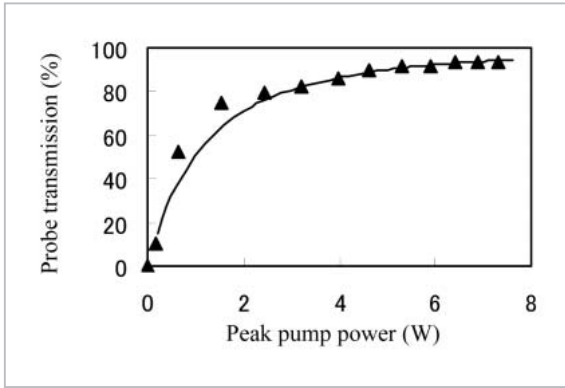


Fig. 13 Modulation depth of the probe signal as a function of peak-coupled pump powers

achievable modulation became saturated at higher pump powers which are due to the pump depletion.

By using the ultrafast recovery time of the silicon optical switch, we developed an optical logic NOR gate. The operation principle and experimental schematic of NOR gate based on the nonlinear transmission curve in silicon wire waveguides is shown in Fig. 14(a) and Fig. 14(b). Signal P1 and P2 with same peak power were combined together and coupled into the waveguide. The weak continuous-wave (CW) probe light at waveguide output was cross-modulated by the sum of P1 and P2 based on non-degenerate TPA process. The Boolean NOR operation was achieved in the

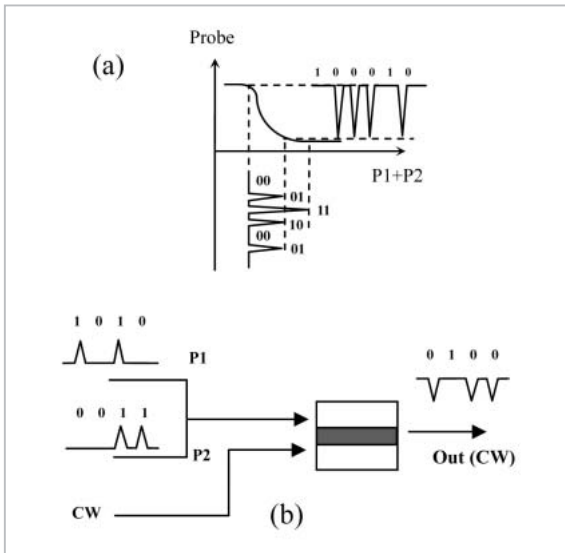


Fig. 14 (a) Operation principle (b) Schematic diagram of NOR gate

form of dark pulses.

Figure 15 shows the experimental demonstration of high speed logic NOR gate using TPA in silicon waveguides. The signal P1 and P2 are shown in Fig. 15(a) and 15(b) respectively. The pulsewidths were both measured to be 1.6 ps FWHM by an autocorrelator. The measured pulses on the sampling oscilloscope were broadened to around 13 ps due to the limited bandwidth of the photodetector. Two signals at different wavelengths were selected to avoid interference and thereby ensure a stable output waveform. The peak powers of P1 and P2 was less than 5 W and corresponding pulse energy was less than 8 pJ. Thus the modulation depth of the output dark pulse is expected to be more than 90%. However, the real modulation depth cannot be measured directly by the limited bandwidth photodetector. It is apparent from Fig. 15(c) that the output logic NOR operation was “0100”. It should be noted that the dark pulse output can easily be avoided if the CW probe light is replaced by pulse train. Since the time separation between two digits was 12.5 ps, the equivalent data-rate of the optical NOR gate was 80 Gbps. In addition, the logic output can be obtained at any arbitrary wavelength range below the bandgap of silicon.

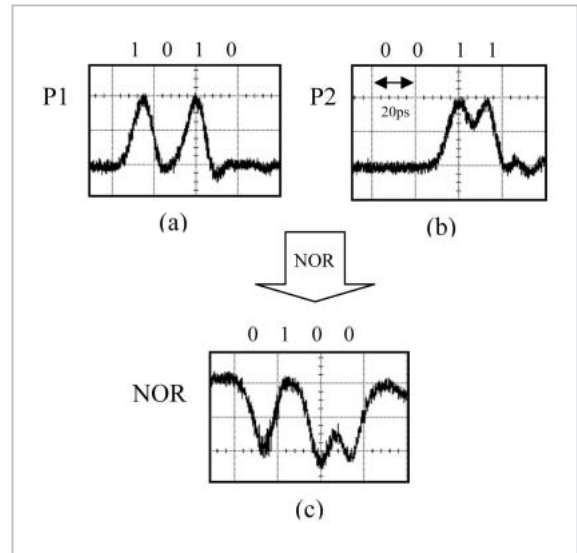


Fig. 15 (a) Signal P1, (b) Signal P2, (c) Output cross-modulated CW probe with logic NOR operation

3.3 Waveguide raman amplifier

Stimulated Raman scattering in silicon [22] was recently shown to have potential for use in an optical amplifier because of the high Raman coefficient and small area of the optical mode in silicon waveguides. However the optical loss introduced by TPA generated free carriers can prevent the realization of net optical gain from SRS in continuous-wave pumped silicon waveguides [23]. One of the attractive features in Raman amplification was that the signal gain spectrum depends on the wavelength of the pumping source. Here we use picosecond pulse pumping (at 1557.4 nm wavelength) to achieve high net optical gain (for 1694.6 nm wavelength probe pulses) as the low pulse duty cycle ensures a low free carrier density in the SOI waveguide.

The waveguide structure for the Raman gain measurements are shown in Fig. 1. The pulse source was a passively mode-locked figure-eight fiber ring laser, which provided pump pulses (1557.4 nm) at repetition rate of 18 MHz and 6.6 ps full-width half maximum pulsewidth. The probe pulses (1694.6 nm, 1 ps) were generated using the well-known soliton self-frequency shift effect in the polarization maintaining fiber (PMF) [24]. In the configuration, the upper path provided pump pulses and amplified by a high-power EDFA, while the lower path provides the probe pulses.

Accurate experimental measurements of the gain were performed on a fiber pigtailed waveguide. Figure 16(a) shows the amplification of the probe pulse at different coupled average pump powers (0, 0.8, 2, 2.9, 3.8, 4.6, 5.3, 6.1, and 7 mW respectively), measured on

the optical spectrum analyzer. The peak-power to average-power ratio of the pump pulses was 7800. Raman gain of 7.8 dB was measured at a coupled average power of 7 mW (55 W peak power). This resulted in a net fiber-to-fiber gain of 6.8 dB for the pigtailed waveguide. As shown in Fig. 16(b), the peak Stokes gain appeared at a frequency shift of 15.6 THz (with linewidth of 96 GHz) from the pump frequency, which agreed with the first order Stokes shift reported previously [25].

The experimentally measured Raman gains (at the peak Stokes wavelength) as a function of average pump power is plotted in Fig. 17. The theoretical curve shows that higher Raman gain (>7.8 dB) is still possible by further increasing the peak pulse power. The gain saturation at high pump powers was due to loss from TPA and its resultant free carriers. A direct time domain measurement of optical amplification from stimulated Raman scattering in the waveguide is shown in the inset of Fig. 17.

4 Summary

We study the nonlinearities in the silicon-on-insulator optical waveguides, which includes two-photon absorption, free-carrier absorption, spontaneous and stimulated Raman scattering. It is experimentally shown that free carriers generated by two-photon absorption in silicon waveguides produce large optical loss.

Several practical silicon based photonic devices have been developed. These include an inexpensive and highly sensitive wave-

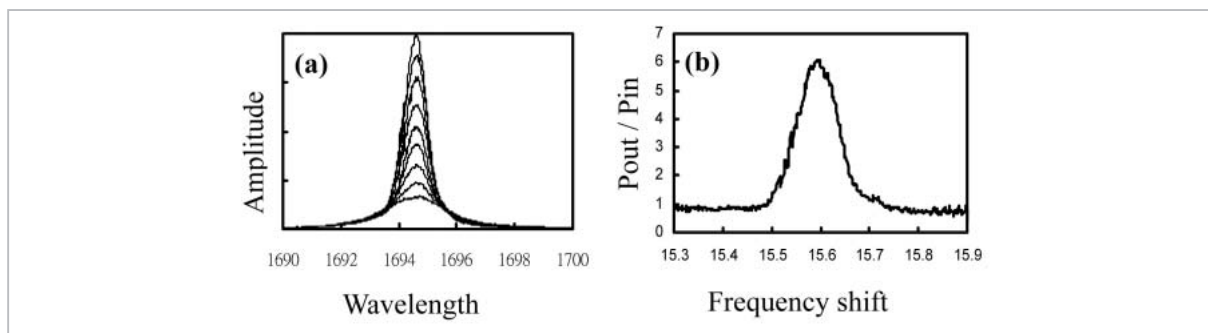


Fig. 16 (a) Raman gain measured on an optical spectrum analyzer, (b) Stokes gain spectrum

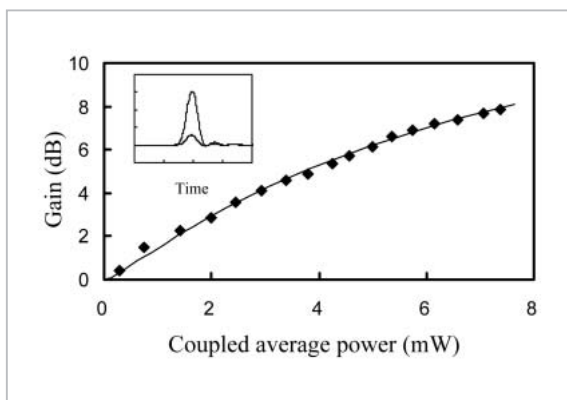


Fig. 17 Experimentally measured Raman gain as a function of coupled average pump powers

guide autocorrelator based on TPA of silicon. The device was easy to fabricate and proved the feasibility of a silicon-based integrated autocorrelator. We also developed a silicon waveguide Raman amplifier which achieves a large optical gain using stimulated Raman scattering in centimeter long devices. An ultrafast all-optical switch using non-degenerate two-photon absorption in a submicron silicon wire waveguide has been demonstrated. Optical probe signal was modulated with less than 3 ps recovery time by short pump pulses with pJ pulse energy. The switching scheme has shown applications in a high speed optical logic NOR gate.

References

- 1 G. T. Reed, "The optical age of silicon", *Nature* 427, 595-596, 2004.
- 2 L. Pavesi, L. Dal Negro, C. Mazzoleni, G. Franzo, and F. Priolo, "Optical gain in silicon nanocrystals", *Nature* 408, 440, 2000.
- 3 N.D. Zakharov, V.G. Talalaev, P. Werner, A.A. Tonkikh, and G.E. Cirlin, "Room-temperature light emission from a highly strained Si/Ge superlattice", *Appl. Phys. Lett.* 83, 3084, 2003.
- 4 R. Claps, D. Dimitropoulos, V. Raghunathan, Y. Han, and B. Jalali, "Observation of stimulated Raman amplification in silicon waveguides", *Opt. Express* 11, 1731 2003.
- 5 R.H. Stolen, E.P. Ippen, "Raman gain in glass optical waveguides", *Appl. Phys. Lett.* 22, 276-278, 1973.
- 6 Richard L. Sutherland, *Handbook of Nonlinear Optics*, Marcel Dekker, New York, 1996.
- 7 H.K. Tsang, R.S. Grant, R.V. Penty, I.H. White, J.B.D. Soole, H.P. LeBlanc, N.C. Andreadakis, E. Colas, and M.S. Kim, "GaAs/GaAlAs Multi-Quantum Well Waveguide For All-Optical Switching At 1.55 μm ", *Elect. Lett.* 27, 1993-1995, 1991.
- 8 H. K. Tsang, R. V. Penty, I. H. White, R. S. Grant, W. Sibbett, J. B. D. Soole, H. P. LeBlanc, N. C. Andreadakis, R. Bhat, and M. A. Koza, "2-photon absorption and self-phase modulation in InGaAsP/InP multi-quantum-well wave-guides", *J. Appl. Phys.* 70, 3992, 1991.
- 9 M. Dinu, F. Quochi, and H. Garcia, "Third-order nonlinearities in silicon at telecom wavelengths", *Appl. Phys. Lett.* 82, 2954-2956, 2003.
- 10 R.A. Soref and B.R. Bennett, "Electrooptical effects in silicon", *IEEE J. Quantum Electron.* 23, 123, 1987.
- 11 J. A. Armstrong, "Measurement of picosecond laser pulse width", *Appl. Phys. Lett.*, 10, 16, 1967.
- 12 Y. Takagi, T. Kobayashi, and K. Yoshihara, "Multiple shot and single shot autocorrelators based on 2-photon conductivity in semiconductors", *Opt. Lett.*, 17, 658, 1992.
- 13 F. R. Laughton, J. H. Marsh, D. A. Barrow, and E. L. Portnoi, "The 2-photon absorption semiconductor wave-guide autocorrelator", *IEEE J. Quantum Electron.*, 30, 838, 1994.
- 14 H. K. Tsang, L. Y. Chan, J. B. D. Soole, H. P. LeBlanc, M. A. Koza, and R. Bhat, "High sensitivity autocorrelation using 2-photon absorption in InGaAsP wave-guides", *Electron. Lett.*, 31, 1773, 1995.
- 15 INRAD model 5-14-LD autocorrelator manual, INRAD International Inc., Northvale, NJ, USA.

-
- 16 K. Kikuchi, "Optical sampling system at 1.5 μ m using two photon absorption in Si avalanche photodiode", Electron. Lett., 34, 1354, 1998.
 - 17 T. Kamiya and M. Tsuchiya, "Progress in ultrafast photonics", Jap. J. Appl. Phys. Part 1 Rev. Papers 44, 5875-5888, 2005.
 - 18 W. Bogaerts, D. Taillaert, B. Luyssaert, P. Dumon, J. Van Campenhout, P. Bienstman, D. Van Thourhout, R. Baets, V. Wiaux, and S. Beckx, "Basic structures for photonic integrated circuits in Silicon-on-insulator", Opt. Express 12, 1583-1591, 2004.
 - 19 V. R. Almeida, C. A. Barrios, R. R. Panepucci, and M. Lipson, "All-optical control of light on a silicon chip", Nature 431, 1081-1084, 2004.
 - 20 R. L. Espinola, J. I. Dadap, R. M. Osgood, Jr., S. J. McNab, and Y. A. Vlasov, "Raman amplification in ultrasmall silicon-on-insulator wire waveguides", Opt. Express 12, 3713-3718, 2004.
 - 21 T. K. Liang and H. K. Tsang, "Role of free carriers from two-photon absorption in Raman amplification in silicon-on-insulator waveguides", Appl. Phys. Lett. 84, 2745-2747, 2004.
 - 22 R. Claps, D. Dimitropoulos, V. Raghunathan, Y. Han, and B. Jalali, "Observation of stimulated Raman amplification in silicon waveguides", Opt. Express 11, 1731-1739, 2003.
 - 23 T.K. Liang and H.K. Tsang, "On Raman gain in silicon waveguides: limitation from two-photon absorption generated carriers", in CLEO'04, CThT poster session San Francisco, 2004.
 - 24 N. Nishizawa and T. Goto, "Widely wavelength-tunable ultrashort pulse generation using polarization maintaining optical fibers", IEEE J. Select. Topics Quantum. Electron. 7, 518-524, 2001.
 - 25 J.M. Ralston and R. K. Chang, "Spontaneous-Raman-scattering efficiency and stimulated scattering in silicon", Phys. Rev. B 2, 1858-1862, 1970.

Liang Tak-Keung, Ph.D.

*former : Expert Researcher, Photonic Information Technology Group, Basic and Advanced Research Department
Shiriconfotonics*

Tsang Hon Ki, Ph.D.

*former : Advanced Communications Technology Group, New Generation Network Research Center
Shiriconfotonics*

Nunes Luis Romeu, Ph.D.

*former : Limited Term Reseacher, Advanced Communications Technology Group, New Generation Network Research Center
Shiriconfotonics*

TSUCHIYA Masahiro, Dr. Eng.

*Group leader, Advanced Communications Technology Group, New Generation Network Research Center (former : Group leader, Photonic Information Technology Group, Basic and Advanced Research Department)
Photonics, Electronics*